Repeat DNA-PAINT suppresses background and non-specific signals in optical nanoscopy

Alexander H. Clowsley[1], William T.Kaufhold[2,3], Tobias Lutz[1], Anna Meletiou[1], Lorenzo Di Michele[3], Christian Soeller[1]*

[1] Living Systems Institute & Biomedical Physics, University of Exeter, Exeter, UK.
[2] Cavendish Laboratory, University of Cambridge, Cambridge, UK.
[3] Department of Chemistry, Molecular Sciences Research Hub, Imperial College London, UK.
* Corresponding author: C.Soeller@exeter.ac.uk

Abstract:

DNA-PAINT is a versatile optical super-resolution technique relying on the transient binding of fluorescent DNA 'imagers' to target epitopes. Its performance in biological samples is often constrained by spurious signals produced by excess imagers. Here we describe Repeat DNA-PAINT, a method that enables a substantial reduction in imager concentration, thus suppressing spurious signals. Additionally, Repeat DNA-PAINT reduces photoinduced target-site loss and can accelerate sampling, all without affecting spatial resolution.

Introduction:

Super-resolution optical microscopy methods have become essential tools in biology, and among these DNA-PAINT[1–5] has proved especially versatile.[6,7] In DNA-PAINT, epitopes of interest are labelled with 'docking' DNA motifs, while dye-modified 'imager' oligonucleotides are introduced in solution. Transient hybridization to docking motifs immobilizes imagers for long enough to generate 'blinks' (events) in a camera frame, which can then be fitted to localize target epitopes with sub-diffraction resolution.[2] DNA-PAINT carries several advantages compared to competing approaches such as STORM[8,9] and PALM,[10,11] eliminating the need for photo- or chemically-switchable dyes and effectively preventing photobleaching, due to fresh imagers continuously diffusing in from the bulk.

The unparalleled flexibility of DNA-PAINT comes at a cost, in the form of a number of serious drawbacks currently limiting the applicability and performance of the technology in real-life biological scenarios. The presence of free imagers produces a diffuse fluorescent background, which compromises event detection and localization precision. The impact of free-imager signals is particularly severe when imaging deep in biological tissues, where efficient background-rejection methods such as TIRF cannot be used. Additionally, imagers often exhibit substantial non-specific binding to biological preparations, which complicates data interpretation[7] and can prevent detection of sparse targets.[12] Both imager-induced background and non-specific events can be reduced by decreasing imager concentration. However, such a reduction also decreases event rates and extends image-acquisition timescales, which is often prohibitive due to limitations in mechanical and chemical sample stability. Finally, despite it being effectively immune to photobleaching, DNA-PAINT has been shown to suffer from photo-induced inactivation of docking strands.[13]

Here we introduce Repeat DNA-PAINT, a straightforward strategy that mitigates all these critical limitations of DNA-PAINT.

Results and Discussion:

As demonstrated in Fig. 1a and c, we employ docking motifs featuring N identical Repeated Domains (NxRD, N = 1, 3, 6, 10) complementary to imagers. Unless otherwise specified, we use a 9-nucleotide (nt) imager (P1) whose concentration is referred to as [I]. Tests performed on functionalized microspheres demonstrate a linear growth in event rate with increasing N, for fixed imager concentration [I] = 50 pM (Fig. 1b). Experimental trends are confirmed by molecular simulations, relying on the oxDNA[14] model and the Forward-Flux Sampling method to estimate imager-docking binding rates[15] (Fig. 1b). Simulations further highlight that imagers bind all individual domains on the repeat-docking motifs with similar probability, proving that the elongation of docking motifs does not hinder their accessibility (Supplementary Fig. 1).

To further verify the linear increase in event rate with N afforded by Repeat DNA-PAINT, we devise a strategy where it can be directly compared to regular DNA-PAINT in biological samples. We labelled ryanodine receptors (RyRs) in cardiac tissue[6] with a common Anchor strand that initially held a 1xRD motif. The latter could then be displaced through a toe-holding reaction, and replaced with a 10xRD strand (Fig. 1c). As expected, we find nearly identical event rates when imaging 1xRD with [I] = 0.4 nM and 10xRD with [I] = 40 pM (Fig. 1d). Importantly, Supplementary Fig. 2 demonstrates that unbound 10xRD needs to be removed to restore event rates.

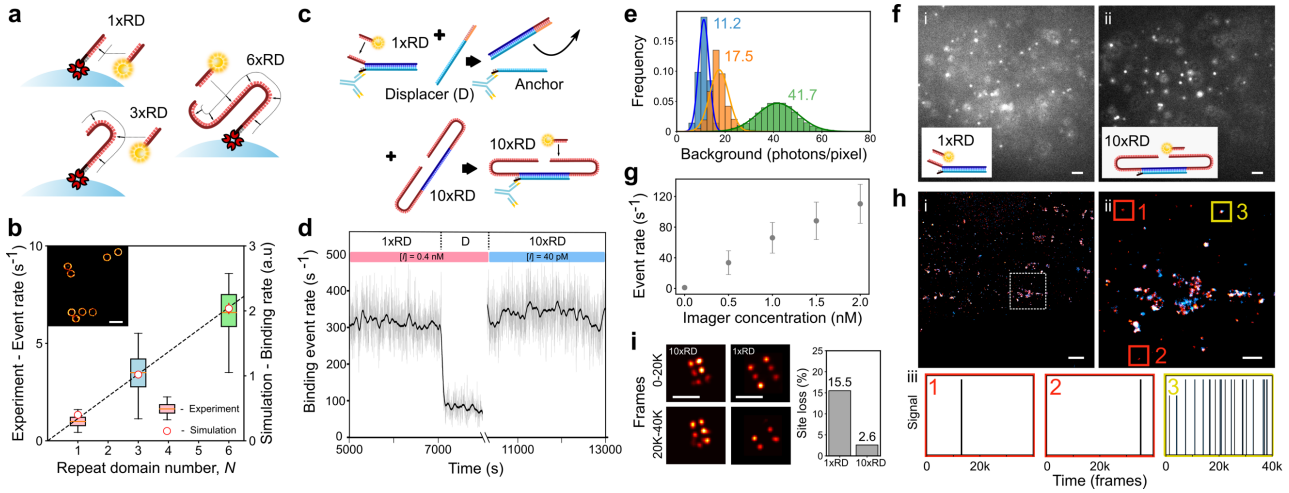

Figure 1. Repeat DNA-PAINT suppresses background signals and prevents photoinduced site loss. a: Docking motifs with N = 1, 3, or 6 binding sites, here biotin-modified and anchored to streptavidin-coated microspheres**. b:** The event rate scales linearly with N, as determined experimentally on microsphere test samples and by coarse-grained computer simulations. The dashed line is a linear fit to the simulation results. Inset: rendered image of the microspheres. **c:** Scheme enabling swapping between 1xRD and 10xRD docking motifs, applied to RyRs in cardiac tissue. A common anchor strand is first connected to a 1xRD strand, which can be removed with a displacer strand D and replaced with a 10xRD motif. **d:** A typical time trace of event-rates recorded in cardiac tissue using the scheme in **c**. Event-rates remain approximately unchanged when probing 1xRD with imager concentration [I] = 0.4 nM and 10xRD motifs with [I] = 40 pM. Gray: event rates for every frame. Black: 50-frame running average. **e:** Histograms of background number of photons/pixel in cardiac tissue with no imager present (blue), [I] = 0.04 nM (orange) and [I] = 0.4 nM (green). Mean photon numbers are indicated. **f:** Raw camera frames of cardiac tissue labelled for RyRs and recorded using 1xRD with [I] = 0.4 nM (**i**), and then 10xRD with [I] = 40 pM (**ii**), using the scheme in **c**. Note the lower background and better contrast in (**ii**). **g:** Rate of non-specific binding events of P1 imagers to unlabelled cardiac tissue as a function of [I], displaying a linear trend. **h:** (**i**) Two-channel DNA-PAINT image of RyRs obtained using the protocol in **e** and rendering 1xRD/10xRD events in red/cyan. (**ii**) A magnified view of the boxed region in (**i**). (**iii**) Time traces of typical 1xRD non-specific (1,2) and specific events (3) from regions highlighted in (**ii**). Note that the specific event (3) also displays 10xRD signal. **i:** Photoinduced site loss as quantified with DNA origami tiles labelled with 10xRD or 1xRD by comparing the number of sites detected in the first half (0-20K frames) versus the second half (20-40K frames) of an experimental run. (left) Rendered images of typical tiles. (right) Histogram summarising the percentage of lost sites, which is much more extensive in 1xRD. Scale bars: **b** 1 μm, **f** 2 μm, **h** (i) 1 μm, (ii) 250 nm, **i** 100 nm.

The ability of Repeat DNA-PAINT to function optimally with a substantial (up to 10-fold) reduction in imager concentration (see also Supplementary Note 1) makes it ideal for mitigating the aforementioned issues, the most direct being the fluorescent background produced by unbound imagers.

In Fig. 1e we quantify the fluorescent background for the cardiac tissue samples in the absence of any imager, for [I] = 0.4 nM while targeting 1xRD, and for [I] = 0.04 nM while imaging with 10xRD. When accounting for the intrinsic (imager-free) signal (11.2 ± 0.3 photons/pixel), the average imager-induced background decreased from 30.5 ± 0.05 photons/pixel at [I] = 0.4 nM to 6.3 ± 0.04 photons/pixel at [I] = 0.04 nM, a ~5-fold reduction. Note that despite the average imager-induced backgrounds did not decrease proportionally to [I], the pixel-value distribution becomes significantly narrower upon reducing imager concentration. Indeed, readings as high as ~50 photons/pixel are not uncommon at [I] = 0.4 nM close to 10x the typical backgrounds recorded with [I] = 0.04 nM. The reduction in background is clearly visible in example frames shown in Fig. 1f-i (1xRD) and Fig. 1f-ii (10xRD), to an extent that substantially improves the detectability of individual binding events and their localization precision[16] (Supplementary Fig. 3).

We then assess the impact of Repeat DNA-PAINT on non-specific imager-binding events at unlabeled locations of complex biological samples, producing spurious blinks that often cannot be distinguished from proximal specific signals. Expectedly, Fig. 1g shows that the rate of non-specific events, as detected in unlabeled cardiac tissue, scales linearly with [I]. Similar trends are observed for different imager sequences (Supplementary Fig. 4). In Fig. 1h we compare the prominence of non-specific events while imaging RyR in cardiac tissue with conventional (1xRD) and Repeat (10xRD) DNA-PAINT, adopting the labeling scheme in Fig. 1c. We observe several non-specific events with 1xRD at [I] = 0.4 nM (i), which are far (10 times) less common when targeting 10xRD at [I] = 0.04 nM (ii).

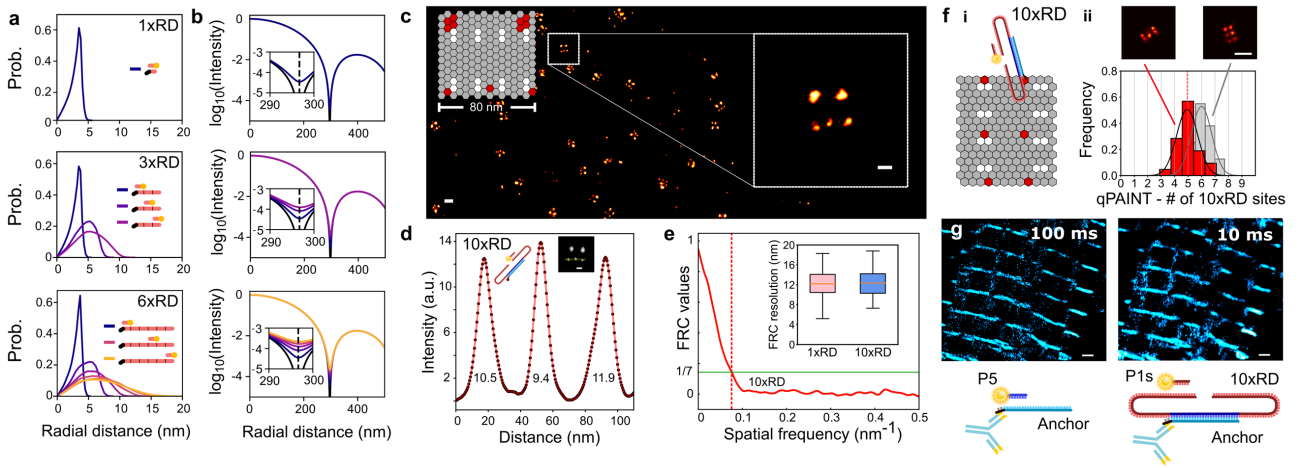

Figure 2. Repeat DNA-PAINT preserves spatial resolution, increases imaging rate and is compatible with qPAINT. a: Simulated radial distributions of the fluorophore site on imagers hybridized to all possible sites on 1xRD, 3xRD and 6xRD, with respect to the anchoring point of the docking motif. **b:** Radial profiles of blinks as obtained by convolving the fluorophore-distributions in **g** with the microscope point-spread function (Supplementary Fig. 6). Insets: zoom in of the region around the first Airy minimum, showing very small broadening that is unlikely to be experimentally detectable. **c:** Scheme of DNA-origami test tiles with red sites indicating the locations of 10xRD motifs and a rendered DNA-PAINT image. **d:** Typical spatial profiles measured across the 'spots' of origami tiles with 10xRD strands as in **c,** with full-width at half maximum (FWHM) spot diameters as indicated. The average FWHM is 12.3 ± 1.8 nm (mean ± SD), nearly identical to 12.6 ± 2.1 nm determined for 1xRD (Supplementary Fig. 7). **e:** Fourier Ring Correlation (FRC) resolution measurements of DNA-PAINT images of origami tiles with 1xRD strands (12.12 ± 2.69 nm, mean ± SD) are indistinguishable from 10xRD (12.36 ± 2.67 nm). **f:** (**i**) Scheme of the origami test tile used for qPAINT experiments. Due to natural self-assembly inaccuracy, not all tiles feature 6 detectable docking sites. (**ii**) Distribution of the number of docking sites determined from qPAINT in tiles featuring 5 detectable sites (red). The median of the histogram is 4.93 ± 0.16 sites/tile. The grey histogram indicates qPAINT results for tiles with 6 sites, used for calibration. Top: rendered images of representative tiles. **g:** Rendered DNA-PAINT images of RyRs in cardiac tissue as imaged with regular DNA-PAINT (1xRD) at low frame-rate (100 ms/frame, left), and Repeat DNA-PAINT (10xRD) at high frame-rate (10 ms/frame, right), showing similar results. The overall image acquisition time was 2000 s for 1xRD and 1600 s for 10xRD (Supplementary Fig. 8). Samples with 1xRD were imaged with 9 nt P5 imagers. Shorter (8 nt) imagers were used with 10xRD to achieve brief binding times and avoid spatiotemporal overlap of the blinks (see also Supplementary Note 1). In both cases, we used [*I*] ~ 0.3 nM. Scale bars: **c** 100 nm, **c** and **d** inset 30 nm, **f** 100 nm, **g** 1 μm.

To distinguish specific from non-specific events in these datasets we relied on their qualitatively different kinetic behavior. While specific binding occurs steadily in labelled regions (Fig. 1h, inset 3), non-specific events are often localized in time[1] (Fig. 1h, insets 1,2). Although occasionally applicable, this identification strategy is only robust if specific and non-specific binding sites are spatially isolated as for the present case, in which RyRs form compact patterns. In samples where docking-strand density is higher and more uniformly distributed non-specific events cannot be easily separated (Supplementary Fig. 5), introducing artefacts in the reconstructed images and potentially distorting site-counting as performed *e.g. via* qPAINT.[3] Repeat DNA-PAINT offers, in turn, a robust route for suppressing spurious events independent of sample characteristics.

Despite its insensitivity to photobleaching, DNA-PAINT is subject to a progressive inactivation of docking sites, ascribed to their interaction with the free-radical states of photo-excited fluorochromes.[13] The domain redundancy in Repeat PAINT can greatly slow down site loss, as we confirmed with origami test samples. For tiles with 1xRD and 10xRD motifs, we compare the number of sites detected in the first 20K frames of long imaging runs, to those counted in the following 20K frames. While for 1xRD tiles we observed a ~15.5% loss of docking sites, 10xRD tiles just lose ~2.6% (Fig. 1i), a 5-fold suppression.

A potential issue deriving from the extension of the docking strands is the loss of spatial resolution,[17,18] as the flexible docking-imager complexes undergo rapid thermal fluctuations during binding events (see Supplementary Note 2). We use oxDNA simulations to quantify the resulting 'blurring', by sampling the distance between the tethering point of the docking strand and the fluorophore location of imagers hybridized to each binding site in 1xRD, 3xRD, and 6xRD motifs. The results, summarized in Fig. 2a, demonstrate narrow fluorophore distributions for the binding sites closest to the tethering point, and broader ones for the more distal sites, peaked at ~8 nm for the furthest domain. Although these broadenings may appear significant compared to the resolution of DNA-PAINT in optimal conditions (~5 nm[19]), they have little impact on the precision with which one can localize the labelled epitope by fitting the diffraction-limited image of a blink. The effect can be quantified by convolving the fluorophore distributions (Supplementary Fig. 6 and Supplementary Note 2) with the theoretical point-spread function (PSF) of the microscope, as shown in Fig. 2b. The PSF broadening is minute and produces, at most, a 0.15% shift in the location of the first Airy minimum.

We thus do not expect any loss of experimental resolution, a prediction that we confirmed on DNA-origami test samples (Fig. 2c), showing no detectable resolution difference between 1xRD and 10xRD, both rendering spots with apparent diameter of ~12 nm (Fig. 2d and Supplementary Fig. 7). Similarly, the Fourier Ring Correlation (FRC) measure of resolution[20] was essentially unaltered between 1xRD (12.2 ± 2.7 nm) and 10xRD (12.4 ± 2.7 nm) images, as shown in Fig. 2e.

Repeat DNA-PAINT is also fully compatible with extensions of DNA-PAINT, such as qPAINT, a technique that estimates the number of available docking sites within a region of interest. We confirm the accuracy of qPAINT with origami tiles displaying 5 10xRD motifs, where the technique estimates 4.93 ± 0.16 sites/tile (Fig. 2f, and SI Methods).

Finally, we point out that the boost in event-rate afforded by Repeat DNA-PAINT can also be exploited to increase acquisition rate. Fig. 2g demonstrates that by simply replacing 1xRD with 10xRD at "conventional" imager concentration ([*I*] ~ 0.3 nM) one can increase frame rate 10-fold, and reduce overall imaging time ~6-fold, an acceleration which could easily be further improved by optimizing illumination conditions (Supplementary Fig. 8).

Conclusions:

In summary, we demonstrate that Repeat DNA-PAINT mitigates all key limitations of DNA-PAINT, namely non-specific events (10x reduction), free-imager background (5x reduction) and photoinduced site loss (5x reduction) while also being able to accelerate data acquisition. The implementation of Repeat DNA-PAINT is straightforward and does not carry any known drawbacks, it is routinely applicable, consolidating the role of DNA-PAINT as one of the most robust and versatile SMLM methods.

Supporting information:

Supporting information includes experimental methods and materials, simulation methods, supplementary figures, tables and notes.

Acknowledgements and funding:

We thank Dr. Ruisheng Lin for his assistance with PyME software control. This work was supported by the Engineering and Physical Sciences Research Council of the UK (No. EP/N008235/1) and Biotechnology and Biological Sciences Research Council Grants BB/P026508/1 and BB/T007176/1. LDM acknowledges funding from a Royal Society University Research Fellowship (UF160152) and from the European Research Council (ERC) under the Horizon 2020 Research and Innovation Programme (ERC-STG No 851667 — NANOCELL). WTK acknowledges funding from an EPSRC DTP studentship. This work was performed using resources provided by CSD3 operated by the University of Cambridge Research Computing Service (www.csd3.cam.ac.uk), provided by Dell EMC and Intel using Tier-2 funding from the EPSRC (capital grant EP/P020259/1), and DiRAC funding from STFC (www.dirac.ac.uk).

Author contributions:

C.S & L.D.M supervised the research progress. Data acquisition was performed by A.H.C, T.L, W.T.K, A.M and data analysis was performed with contributions from all authors. T.L prepared and imaged microspheres, W.T.K made the origami tiles, A.H.C & T.L prepared and imaged the origami tiles, A.H.C & A.M prepared and imaged biological samples. Simulations and modelling were developed by W.T.K & L.D.M. The manuscript was written by A.H.C, W.T.K, L.D.M, C.S and all authors reviewed the manuscript.

Competing interests:

The authors declare no competing interests in the work presented.

References:

1. Jungmann, R. *et al.* Multiplexed 3D cellular super-resolution imaging with DNA-PAINT and Exchange-PAINT. *Nat. Methods* **11**, 313–318 (2014).
2. Schnitzbauer, J., Strauss, M. T., Schlichthaerle, T., Schueder, F. & Jungmann, R. Super-resolution microscopy with DNA-PAINT. *Nat. Protoc.* **12**, 1198–1228 (2017).
3. Jungmann, R. *et al.* Quantitative super-resolution imaging with qPAINT. *Nat. Methods* **13**, 439–442 (2016).
4. Schueder, F. *et al.* Multiplexed 3D super-resolution imaging of whole cells using spinning disk confocal microscopy and DNA-PAINT. *Nat. Commun.* **8**, 1–9 (2017).
5. Gómez-García, P. A., Garbacik, E. T., Otterstrom, J. J., Garcia-Parajo, M. F. & Lakadamyali, M. Excitation-multiplexed multicolor superresolution imaging with fm-STORM and fm-DNA-PAINT. *Proc. Natl. Acad. Sci.* **115**, 12991–12996 (2018).
6. Jayasinghe, I. *et al.* True Molecular Scale Visualization of Variable Clustering Properties of Ryanodine Receptors. *Cell Rep.* **22**, 557–567 (2018).

7. Böger, C. *et al.* Super-resolution imaging and estimation of protein copy numbers at single synapses with DNA-point accumulation for imaging in nanoscale topography. *Neurophotonics* **6**, 035008 (2019).
8. Rust, M. J., Bates, M. & Zhuang, X. Sub-diffraction-limit imaging by stochastic optical reconstruction microscopy (STORM). *Nat. Methods* **3**, 793–795 (2006).
9. Heilemann, M. *et al.* Subdiffraction-resolution fluorescence imaging with conventional fluorescent probes. *Angew Chem Int Ed* **47**, 6172–6176 (2008).
10. Betzig, E. *et al.* Imaging intracellular fluorescent proteins at nanometer resolution. *Science* **313**, 1642–1645 (2006).
11. Hess, S. T., Girirajan, T. P. K. & Mason, M. D. Ultra-high resolution imaging by fluorescence photoactivation localization microscopy. *Biophys. J.* **91**, 4258–4272 (2006).
12. Geertsema, H. *et al.* Left-handed DNA-PAINT for improved superresolution imaging in the nucleus. *bioRxiv* 2020.03.28.010553 (2020) doi:10.1101/2020.03.28.010553.
13. Blumhardt, P. *et al.* Photo-Induced Depletion of Binding Sites in DNA-PAINT Microscopy. *Molecules* **23**, 3165 (2018).
14. Ouldridge, T. E., Šulc, P., Romano, F., Doye, J. P. K. & Louis, A. A. DNA hybridization kinetics: zippering, internal displacement and sequence dependence. *Nucleic Acids Res.* **41**, 8886–8895 (2013).
15. Ouldridge, T. E., Louis, A. A. & Doye, J. P. K. Structural, mechanical, and thermodynamic properties of a coarse-grained DNA model. *J. Chem. Phys.* **134**, 085101 (2011).
16. Mortensen, K. I., Churchman, L. S., Spudich, J. A. & Flyvbjerg, H. Optimized localization analysis for single-molecule tracking and super-resolution microscopy. *Nat. Methods* **18**, 377–381 (2017).
17. Sahl, S. J., Hell, S. W. & Jakobs, S. Fluorescence nanoscopy in cell biology. *Nat. Rev. Mol. Cell Biol.* **18**, 685–701 (2017).
18. Ries, J., Kaplan, C., Platonova, E., Eghlidi, H. & Ewers, H. A simple, versatile method for GFP-based super-resolution microscopy via nanobodies. *Nat. Methods* **9**, 582–584 (2012).
19. Schlichthaerle, T. *et al.* Direct Visualization of Single Nuclear Pore Complex Proteins Using Genetically-Encoded Probes for DNA-PAINT. *Angew. Chem. Int. Ed.* **58**, 13004–13008 (2019).
20. Nieuwenhuizen, R. P. J. *et al.* Measuring image resolution in optical nanoscopy. *Nat. Methods* **10**, 557–562 (2013).